frontiers | Frontiers in Physics

TYPE Original Research
PUBLISHED 20 October 2022
DOI 10.3389/fphy.2022.1009421

OPEN ACCESS

EDITED BY
Daniele Dell'Aquila,
University of Sassari, Italy

REVIEWED BY
Magda Cicerchia,
University of Padua, Italy
Libertad Barrón-Palos,
Universidad Nacional Autónoma de México, Mexico

*CORRESPONDENCE
Neven Soić,
soic@irb.hr

SPECIALTY SECTION
This article was submitted to Nuclear Physics,
a section of the journal
Frontiers in Physics

RECEIVED 01 August 2022
ACCEPTED 29 September 2022
PUBLISHED 20 October 2022

CITATION
Vukman N, Soić N, Freer M, Alcorta M, Connolly D, Čolović P, Davinson T, Di Pietro A, Lennarz A, Psaltis A, Ruiz C, Uroić M and Williams M (2022), Cluster decays of ^{12}Be excited states.
Front. Phys. 10:1009421.
doi: 10.3389/fphy.2022.1009421

Cluster decays of ^{12}Be excited states

Nikola Vukman[1], Neven Soić[1]*, Martin Freer[2], Martin Alcorta[3], Devin Connolly[3], Petra Čolović[1], Thomas Davinson[4], Alessia Di Pietro[5], Annika Lennarz[3], Athanasios Psaltis[6], Chris Ruiz[3], Milivoj Uroić[1] and Matthew Williams[3]

[1]Ruđer Bošković Institute, Zagreb, Croatia, [2]University of Birmingham, Birmingham, United Kingdom, [3]TRIUMF, Vancouver, BC, Canada, [4]University of Edinburgh, Edinburgh, United Kingdom, [5]INFN Laboratori Nazionali del Sud, Catania, Italy, [6]McMaster University, Hamilton, ON, Canada

An experimental study of the helium-cluster decays of the ^{12}Be excited states has been performed using the ^{9}Li + ^{7}Li → α + α + ^{8}He and ^{9}Li + ^{7}Li → α + ^{6}He + ^{6}He reactions at the ^{9}Li beam energy of 74.8 MeV. At excitation energies between 10 and 25 MeV, the ^{12}Be excited states decaying into the ^{4}He + ^{8}He, ^{6}He + ^{6}He, and ^{6}He + ^{6}He*(1.8 MeV, $J^{\pi} = 2^{+}$) have been observed. Most of the observed states decaying into the ^{4}He + ^{8}He and ^{6}He + ^{6}He correspond to previously reported states. The decay to the ^{6}He + ^{6}He*(1.8 MeV, $J^{\pi} = 2^{+}$) channel has been observed for the first time. Two of the five states observed in this new decay channel are also observed in the ground state channel ^{6}He + ^{6}He, while two may correspond to the ^{4}He + ^{8}He decaying states. The states around 13.5 and 20.0 MeV decay to the ^{6}He + ^{6}He and ^{4}He + ^{8}He channels, while the state around 22.3 MeV decays into all three decay channels examined. This experiment is complementary to all previous studies of the ^{12}Be cluster states because of the different reaction mechanisms used for the population of the ^{12}Be cluster states. The observation of the states at high excitations with these exotic decay properties strongly supports the molecular structure of the ^{12}Be excited states.

KEYWORDS

nuclear structure, helium clustering, nuclear molecule, ^{12}Be, neutron-rich light nuclei, transfer reactions, radioactive ion beam

1 Introduction

Detailed data on the properties of nuclei away from the stability line are essential to improve the understanding of nuclear structure and reaction mechanisms. In light nuclei, both aspects of nuclear structure, single-particle dynamics, and nucleon correlations, which result in clustering, are the most pronounced due to the small number of important degrees of freedom. Understanding the correlations and formation of clusters is closely related to fine details of the nuclear force as well as to spatial and quantum symmetries within the nuclei. Modern nuclear theories are able to realistically model A < 20 nuclei starting from individual nucleons and basic principles, making possible detailed comparisons of calculated nuclear properties with the results of phenomenological

approaches and high precision experimental data [1]. To benchmark these models, it is of prime importance to obtain experimental data for the key light nuclei.

The key nuclei to understand α-clustering are beryllium and carbon isotopes. The ^{8}Be and ^{12}C low excitation level schemes correspond to ones for an assembly of two and three α-particles, respectively. The structure of heavier beryllium and carbon isotopes, as well as the effects of additional neutrons to these cluster structures is currently not fully understood. Nuclear molecules are one of the quite exotic structural phenomena discovered away from the stability line [2, 3]. A nuclear molecule is a system built from α-clusters and valence neutrons residing in the orbitals which can be constructed as linear combinations of orbitals around the individual α-particles. The covalent exchange of the neutrons between the α-cores increases the stability of the system, similar to the binding of covalent atomic molecules. The two-center nuclear molecular structures have been identified in ^{9}Be [4–6] and ^{10}Be [7–9]. To establish the nuclear molecule as a general type of structure in neutron-rich nuclei, it is essential to experimentally confirm it in heavier beryllium nuclei, particularly in the ^{12}Be nucleus in which four valence neutrons may occupy shell model orbitals, atomic-like orbitals around individual α-core, or molecular-like orbitals around both α-cores [10].

The experimental results on the cluster decays of the ^{12}Be excited states are very limited and often inconsistent. The earliest measurements of the ^{12}Be projectile inelastic breakup [11–14] provided evidence for a number of states decaying into the ^{4}He + ^{8}He and ^{6}He + ^{6}He clusters. The estimated spins of some of the observed states indicated that they are members of a rotational band of a deformed, exotic ^{6}He + ^{6}He cluster structure in ^{12}Be, which may be linked to an α-4n-α molecule [12, 13]. This molecular rotational band was not confirmed in later measurement of the ^{12}Be inelastic breakup at higher beam energy [15]. The excitation energy spectra for both helium-cluster decay channels obtained in this work show fewer structures than the ones in [12, 13] with a large background of unclear origin. Both experiments used a composite CH_2 target and events originating from different target components were not fully distinguished. This introduced a large uncertainty in the reconstructed ^{12}Be excitation energy spectra in both of these experiments. Although spectra for the assumed reaction on the hydrogen show structures identified as the ^{12}Be excited states, spectra for the reaction on carbon are largely structureless. The most recent measurement of the ^{12}Be breakup off the ^{12}C target [16, 17] at the beam energy similar to one in [12] identified new states close to each helium-cluster decay threshold and provided results in agreement with [12, 13] in the overlapping low excitation energy region. These results are interpreted as confirmation of the proposed molecular rotational band and evidence for a well-developed cluster structure in ^{12}Be. Another experimental approach used to examine the cluster structure of the ^{12}Be excited states is the measurement of the ^{8}He + ^{4}He resonant scattering using a radioactive ^{8}He beam on a thick ^{4}He gas target [18]. The obtained results did not improve the understanding of the ^{12}Be cluster structure as no sharp resonances were observed in the reconstructed ^{12}Be excitation energy spectra for both ^{8}He + ^{4}He and ^{6}He + ^{6}He decay channels in the measured excitation energy range from 13.7 to 16.4 MeV.

From the theoretical side, the structure of the ^{12}Be excited states above the thresholds for their decay into the ^{4}He + ^{8}He (8.9 MeV), ^{6}He + ^{6}He (10.1 MeV), and ^{5}He + ^{7}He (12.4 MeV) has attracted significant interest as an excellent candidate to characterize the evolution of exotic clustering with the addition of neutrons. Some of the recent studies use the no-core shell model (NCSH) [19], the generalized two-center cluster model (GTCM) [10, 20–22], the microscopic generator-coordinate method and complemented NCSM calculations [23], and the antisymmetrized molecular dynamic (AMD) model [24]. The common result of all of these calculations is a well-developed cluster structure with states possessing the ^{4}He + ^{8}He and ^{6}He + ^{6}He structure and grouped into various rotational bands. Another important result is the stabilization of the classical α-cluster structure by excess neutrons. These exotic clustering modes, together with the breakdown of the N = 8 shell closure required to understand the structure of the ground and low-lying excited states [25, 26], set the ^{12}Be nucleus as a key neutron-rich system to benchmark newly developed theoretical models, and improve the knowledge of nuclear structure.

This study reports the results of the experiment using an approach different from all previous studies of clustering in ^{12}Be. This method, resonant particle spectroscopy measurements of many-nucleon or cluster transfer reactions, was successfully applied in earlier research on the clustering in light nuclei close to the stability line. For example, it was applied in previous studies of clustering in ^{10}Be using the ^{7}Li + ^{7}Li $\rightarrow \alpha + \alpha + ^{6}$He reaction, which led to the first observation of the ^{6}He decay of the ^{10}Be excited states [9]. The ^{7}Li nucleus has prominent α + t cluster structure in the ground state ($J^{\pi} = 3/2^{-}$) with clusters being in $l = 1$ relative motion, making it a perfect system for the triton transfer reactions. Two additional neutrons in the ^{9}Li reduce clustering of its ground state ($J^{\pi} = 3/2^{-}$) compared to the ^{7}Li. The overall ^{9}Li + ^{7}Li system has large excess of neutrons (N/Z = 5/3) making this reaction suitable for the study of the neutron-rich light nuclei. In addition, the reaction ^{9}Li + ^{7}Li $\rightarrow \alpha + ^{12}$Be has a large positive Q-value of 12.36 MeV, making it especially suitable for the study of excited states at high ^{12}Be excitations. This experiment is complementary to all previous studies of the ^{12}Be cluster states since it uses the different reaction mechanisms to populate the ^{12}Be cluster states: the expected main reaction mechanisms are triton transfer from ^{7}Li to ^{9}Li and t + 2n transfer from ^{9}Li to ^{7}Li. These transfer reactions may populate exotic molecular structures such as the ones proposed in [20].

2 Experimental details and data analysis

The experiment was performed at the ISAC-II rare-isotope ion beam facility at TRIUMF in Vancouver using the ^{9}Li beam of

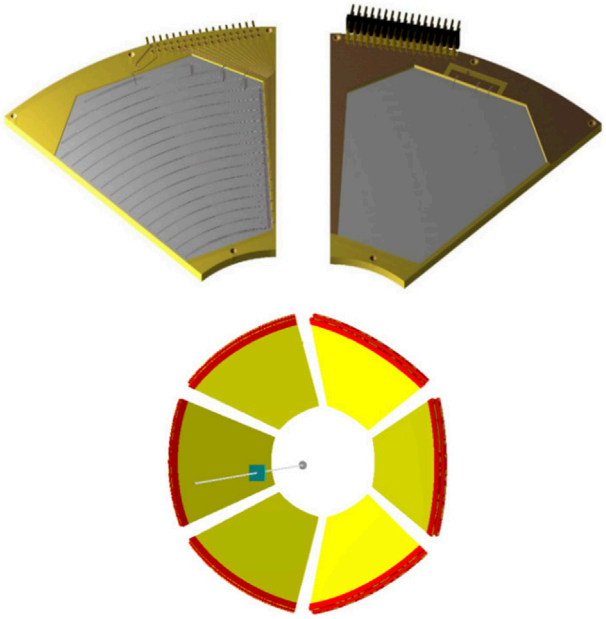

FIGURE 1
Schematic presentation of the LAMP detector telescope setup used in the experiment.

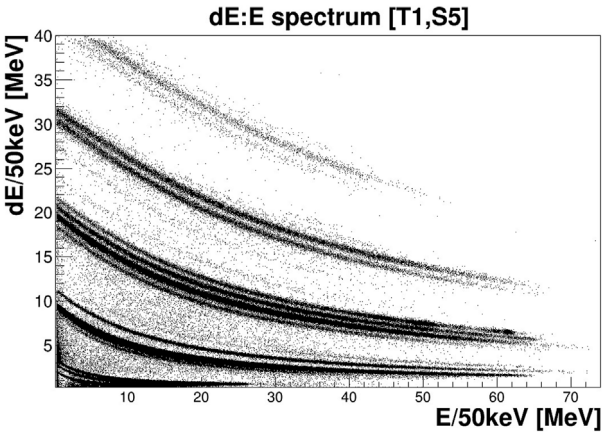

FIGURE 2
Typical particle identification of ΔE−E spectrum obtained for one strip in the E detector: here, the spectrum for strip 5 of telescope T1 is shown. Observed loci correspond to the (from bottom to top) ^{1,2,3}H, ^{3,4,6,8}He, ^{6,7,8,9}Li, ^{7,9,10,11,12}Be, and ^{10,11,12}B.

energy of 74.8 MeV and LiF targets of thickness of ≈ 1 mg/cm^2. The average beam intensity during the 6 days of the measurement was ≈4 × 10^6 pps. No beam contaminants were observed in the recorded data. The beam was focused through a set of collimators resulting in the spot size on the target of < 3 mm diameter. The LiF targets, with natural lithium, were evaporated on thin (≈40 μg/cm^2) Al backing.

The reaction products were detected using a large solid angle silicon strip detector array assembled of six wedge-shaped telescopes, each having a ΔE detector of thickness ≈70 μm and E detector of thickness ≈1.5 mm, arranged in a "lampshade" geometry which covered an azimuthal angle of 360° (Figure 1). Both ΔE and E detectors were single-sided strip detectors with 16 circular strips of 5 mm wide separated by 100 μm of SiO_2, specifically YY1 design made by Micron Semiconductor Ltd. [27]. The polar angular range covered by the detector array was from 16.6° to 47.8° with an angular resolution of ≈2°. The resolution in the azimuthal angle was ≈ 55°, defined by the active area of each of the six segments. The reaction products were identified using the ΔE–E technique, with excellent isotope separation from hydrogen to boron nuclei (Figure 2). Energy calibration of all detectors was performed using an α-source containing ^{239}Pu, ^{241}Am, and ^{244}Cm isotopes with α energies of 5.155, 5.486, and 5.805 MeV, respectively. An additional point for the calibration of the E detectors was obtained by measuring the elastic scattering of the ^{9}Li beam of energy 74.8 MeV off a gold target. Two sets of calibration data were taken. The first dataset had only E detectors mounted, and it provided high-quality data for the calibration of the E detectors. The second dataset was taken with both ΔE and E detectors in place, and it was used for the calibration of the ΔE detectors using the α-particles from the source which stopped in the ΔE detectors. This procedure provided high-quality data for the calibration of both detector sets. Elastic scattering data on the gold target were also used for fine corrections of the experimental setup geometry. The detector array was mounted in the TUDA scattering chamber [28] in the ISAC-II hall. Standard electronics for processing signals from the silicon strip detectors were used and data were recorded in the single mode, where every hit in the E detectors above the set thresholds triggered the reading of all ADCs, and the event was recorded.

The kinematically complete measurements of the following reactions were performed to examine the helium-cluster decays of the ^{12}Be excited states:

$$^9Li + ^7Li \rightarrow \alpha + ^{12}Be^* \rightarrow \alpha + \alpha + ^8He, Q = 3.402MeV, \quad (1)$$

$$^9Li + ^7Li \rightarrow \alpha + ^{12}Be^* \rightarrow \alpha + ^6He + ^6He, Q = 2.253MeV. \quad (2)$$

The reaction products were detected in coincidence events and each detected product was identified using graphical cuts imposed on the ΔE–E plots such as the one presented in Figure 2. Coincident detection of two out of the three reaction products allows the reaction exit channel identification and consequently a full kinematical reconstruction of the event by the application of momentum and energy conservation. From the measured energies in the ΔE and E detectors for each identified nucleus, its energy in the reaction was reconstructed accounting for all

possible energy losses in the target and inactive layers of the detectors. A detailed hit reconstruction was also performed by taking into account the geometrical overlap of the strips in the ΔE and E detectors, as well as the signal sharing between two adjacent strips in the detectors. A careful reconstruction of double hits in adjacent strips was also performed in the data analysis. The calibration, fine-tuning of the detector geometry, and hit reconstruction procedure were verified using the elastic and inelastic scattering of the ^{9}Li beam on ^{7}Li and ^{19}F target components, elastic scattering on ^{27}Al target backing and ^{184}W target contaminant, and the ^{1}H(^{9}Li,^{4}He^{6}He) reaction on the hydrogen target contaminant. The double hit procedure in the case of hits in adjacent and separated strips was verified by reconstructing the ^{8}Be ground state for two detected α-particles in the same detector. All reconstructed excitation energy spectra confirmed that the applied procedures produced correct results and that the experimental setup was stable during all data taking time [29]. The stability of the electronics was validated by location in the raw ADC data of constant amplitude signal generated in a pulser during the full data taking time. As an example, the ^{19}F + ^{9}Li elastic scattering peak for the whole detector array and for all recorded data is at correct energy and has a FWHM of 650 keV. For the same set of data, the ^{7}Li + ^{9}Li elastic scattering peak is at correct energy and has a FWHM of 1.3 MeV. The large FWHM value is due to unresolved contribution of the first excited state of ^{7}Li at 478 keV. The excited states of the ^{19}F [30] and ^{7}Li [31] at low excitations were also correctly reconstructed. Another illustration of the data quality is the ^{8}Be ground state reconstructed from the set of data of triple coincidence events ^{4}He + ^{4}He + ^{6}He detected in the whole detector array and for all taken data which is positioned at the correct energy and has an experimental FWHM of 70 keV.

The reconstructed energy and angular position of the two detected and identified reaction products, under the assumption of the mass of the third, undetected nucleus, determine the energy and emission angle of the third reaction product. The sum of energies of all reaction products is equal to the total energy in the reaction exit channel, from which the reaction Q-value can be calculated. The reaction Q-value was calculated for each recorded coincidence event, and it was used to identify an origin of the event from various possible reactions of the ^{9}Li beam with different target constituents. This procedure relies on the correct identification of the undetected reaction product. For composite targets, such as the one used in this experiment, this may lead to misidentification of the reaction exit channel in the case of strong background contributions and low energy/angular resolution. For this reason, an additional procedure for the identification of the reaction exit channel, independent of the mass of the undetected nucleus, was applied [32]. Two kinematical quantities,

$$\tilde{E} = E_3 - Q = E_p - E_1 - E_2, \tag{3}$$

$$\tilde{P} = \frac{p_3^2}{2m_u}\,(\mathrm{m}_u - \text{atomic mass unit}), \tag{4}$$

$$\tilde{E} = \frac{1}{A_3}\tilde{P} - Q, \tag{5}$$

were calculated for each coincident event and plotted in the so-called Catania plot [32]. In this plot, events from the specific reaction gather in a locus around the line with a slope inversely proportional to the mass number of the undetected nucleus which intersects the ordinate at the negative value of the reaction Q-value (Eq. 5, Figure 3). The selection of the events originating from a particular three-body nuclear reaction was performed using both the calculated Q-value and a graphical cut applied around the reaction line in the Catania plot, in order to remove the background contributions as much as possible.

The aforementioned calculations require knowledge of the relative azimuthal angle between two detected reaction products, which cannot be measured using single-sided strip detectors used in the experiment. Thus, nominal values of the relative azimuthal angle were used in the calculations: for hits in the telescopes on the opposite sides of the beam, labeled as dT = 3 events, the nominal value used was 180°; for hits in telescopes separated by one detector segment, labeled as dT = 2, the nominal value of 120° was used; for hits in two adjacent telescopes (dT = 1), the nominal value was 60°; and for the hits in the same telescope (dT = 0), the nominal value was 0°. Real angular ranges of the relative azimuthal angles are [125°–180°] for dT = 3, [65°–175°] for dT = 2, [5°–115°] for dT = 1, and [0°–55°] for the dT = 0 case.

The large uncertainty in the relative azimuthal angle of the detected reaction products results in a large uncertainty in the reconstructed momentum of the undetected reaction product and degrades the resolution in the reaction Q-value and other kinematical quantities calculated for identification of the reaction. This is especially true for the dT = 2 and dT = 1 events. Consequently, for reaction exit channels with Q-values differing by less than 2.5 MeV in dT = 1, 2 sets of data, a clean separation of the corresponding events was not possible. For this reason, experimental data for each reaction exit channel were compared to detailed Monte Carlo simulations of all reaction channels that may contribute to that set of coincidence events. Monte Carlo simulations were performed using the UNISim MC framework [33] and included a realistic description of the experimental setup with all relevant sources of uncertainties, assuming isotropic formation of the ^{12}Be excited state in the first step of the reaction and its subsequent isotropic decay [29]. The results of these simulations guided the selection of events associated with a particular reaction, minimizing background contributions at the cost of reduced event statistics.

For selected events of the particular reaction exit channel, the relative energy between each pair of the reaction products was calculated, in other words, the excitation energy spectra were reconstructed for all nuclei which are possible pathways to the same exit channel. Since all the reaction products were identified

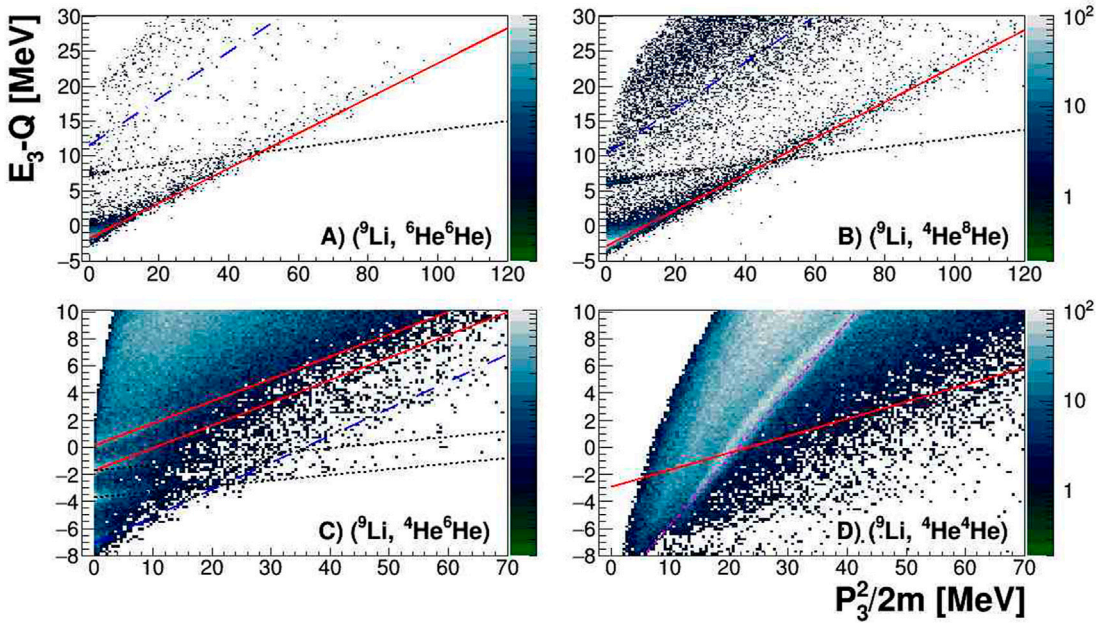

FIGURE 3
Examples of the correlation plots for the identification of events originating from various reaction exit channels: Catania plots reconstructed for the coincident detection of reaction product pairs relevant for the ^{12}Be excited states. The spectra **(A,C)** correspond to the data for the ^{6}He + ^{6}He decay of the ^{12}Be excited states, i.e. reaction (2) with Q value of 2.253 MeV. The spectra **(B,D)** are for the ^{4}He + ^{8}He decay and reaction (1) with Q = 3.402 MeV. In all the cases, reaction products are detected as dT = 3 events. Red lines mark loci associated with the reaction on the ^{7}Li, blue dashed lines on the ^{6}Li, and black dotted lines on the ^{19}F. Additional red and black lines in plot C correspond to undetected ^{6}He in its first excited state at 1.8 MeV for reaction on ^{7}Li, and to undetected ^{18}O in its first excited state at 1.99 MeV for reaction on ^{19}F, respectively. On plot D, intense locus of the events marked with purple line corresponds to the reaction on hydrogen content of the target.

at this stage, it was possible to reconstruct the relative azimuthal angle from energies and polar angles of two detected nuclei. This procedure significantly improves the excitation energy resolution. For wrongly associated events, the relative azimuthal angle, and consequently the excitation energy are incorrect and degrade the spectral resolution, but do not lead to prominent peaks in the spectrum [29]. The excitation energy is obtained by adding the calculated value of the relative energy to the corresponding threshold energy for a particular decay channel. For example, the final state α + α + ^{8}He may have proceeded through the excited states of ^{8}Be decaying into α + α and two possible combinations of the ^{12}Be excited states decaying into α + ^{8}He. The relative energy between detected reaction products depends on their energies, polar angles, and relative azimuthal angle, while the relative energy between one detected and undetected reaction product is calculated using the energy and polar angle of other detected reaction product.

The ^{12}Be excitation energy spectra were reconstructed for two possible helium-cluster decay channels: for the ^{6}He + ^{6}He decay, the ^{4}He + ^{6}He and ^{6}He + ^{6}He coincident events were analyzed and for the ^{4}He + ^{8}He decays, the ^{4}He + ^{8}He and ^{4}He + ^{4}He coincident events were analyzed. All selected events presented in the excitation energy spectra originate from the ^{9}Li + ^{7}Li reaction. The calculated excitation energies for each selected event are plotted in 2D correlation spectra for three possible pairs of reaction products, thus in three 2D spectra in total, of which the most relevant one for a particular set of data are presented in Figure 4. The excited state decaying into the particular pair of nuclei can be identified as a straight locus perpendicular to the corresponding axis. In the ^{4}He + ^{6}He + ^{6}He exit channel, strong background contributions from the ^{10}Be states decaying into the ^{4}He + ^{6}He were observed. These results will be presented in a separate publication. Similarly, the ^{8}Be excited states decaying into two α-particles produced a strong background in the ^{12}Be excitation energy spectra for the ^{4}He + ^{8}He decay. These observed states, known ^{10}Be states at 9.56, 10.15, and 11.76 MeV [34] decaying into the ^{4}He + ^{6}He, and known ^{8}Be states from the ground state up to 20 MeV in excitation [34] decaying into two α-particles, were excellent test samples for quality checks of the data analysis procedure, for verification of the Monte Carlo simulations, and for estimation of the uncertainty and resolution in the ^{12}Be excitation energy. The strongest peaks in these background contributions were excluded from the final ^{12}Be excitation energy spectra by applying cuts on the regions in the 2D correlation spectra which were projected on the ^{12}Be axis. The remaining background contributions in the ^{12}Be excitation

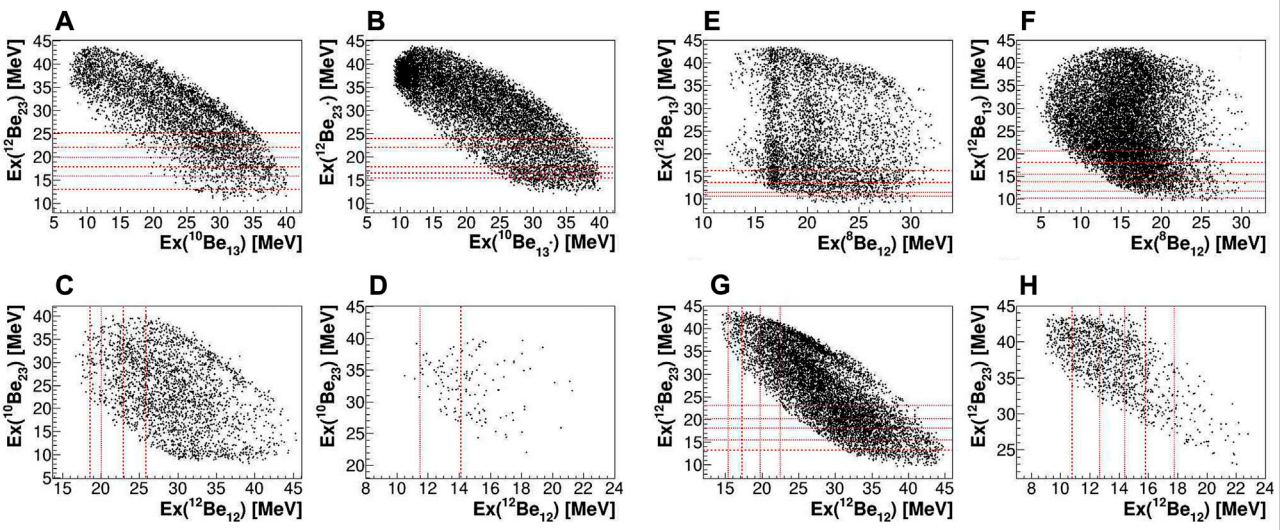

FIGURE 4
Typical correlation plots for the identification of excited states: 2D plots of excitation energy spectra reconstructed for composite systems made of various pairs of the three final reaction products. Plots A, B, C, and D are reconstructed for events associated with the ^{6}He + ^{6}He decay, plots E, F, G, and H for the ^{4}He + ^{8}He decay of the ^{12}Be excited states. Spectra are reconstructed for the ^{4}He + ^{6}He dT = 3 coincidences for undetected ^{6}He in the ground state **(A)** and the first excited state at 1.8 MeV **(B)**; ^{6}He + ^{6}He coincidences for dT = 3 **(C)** and dT = 1 **(D)**; ^{4}He + ^{4}He coincidences for dT = 3 **(E)** and dT = 2 **(F)**; ^{4}He + ^{8}He coincidences for dT = 3 **(G)** and dT = 1 **(H)**. The candidates for the ^{12}Be states are marked with the lines.

energy spectra produce broad structures mainly at large excitation energies.

The data were analyzed and are presented here separately for all types of ^{x}He + ^{y}He coincidence events and for all possible pairs of the detector array segments (dT = 0, 1, 2, 3), since different sets of events span different regions of the ^{12}Be excitation energy, have different uncertainties, and contain different background contributions. The observed peaks in the ^{12}Be excitation energy spectra were fitted with a Gaussian function on the top of smooth background contributions estimated by the polynomial function and, in some cases, broad Gaussian function at higher excitations to account for increased background contributions. The detection efficiency was also taken into consideration in the spectra analysis. Typical examples of the spectra are shown in Figures 5, 6. It can be seen that excitation energy spectra have rather low resolution and that most of the peaks have limited data statistics.

The excitation energy spectra presented have binning of 320 keV, and it was tested that main structures in the spectra are not artifacts of the data presentation by plotting spectra with binnings from 200 to 500 keV. The criteria to interpret the observed peak in the excitation energy spectrum as a candidate for the ^{12}Be excited state are as follows:

- peak observation in the corresponding 2D correlation plots of excitation energies, examples are presented in Figure 4
- peak observation in at least two independent sets of data
- agreement in fit parameters of the state for different datasets: excitation energy difference of less than 350 keV for the low excitations and up to 600 keV for the highest excitations, and the FWHM value difference smaller than 350 keV

The only exception from the last two criteria are the states in the ^{6}He + ^{6}He*(1.8 MeV) decay, because corresponding coincidence events could have been separated from the data for the ^{6}He ground state decay channel only for one dataset, the dT = 3 ^{4}He + ^{6}He coincidences.

The Monte Carlo simulations provided detection efficiency curves for the excitation energy spectra and estimations of the excitation energy resolution. For these purposes, simulated data were analyzed in the same way as experimental data and these values were assigned from the generated spectra. The correctness of the simulations and a quality check of the data filtering criteria were validated by the analysis of the triple coincidence events ^{4}He + ^{6}He + ^{6}He and ^{4}He + ^{4}He + ^{8}He. Because all three reaction products for the reactions on the ^{7}Li target were detected in these events, reaction exit channel identification was background-free and the resolution in the ^{8,10,12}Be excitation energies was superior to the ones for the double coincidence data. Reconstructed spectra for simulated events were in excellent agreement with spectra from the experimental data. However, these subsets of triple coincidence data covered more limited phase space of the three-body reaction, had much lower detection efficiency, and resulted in much lower event statistics than the double coincidence

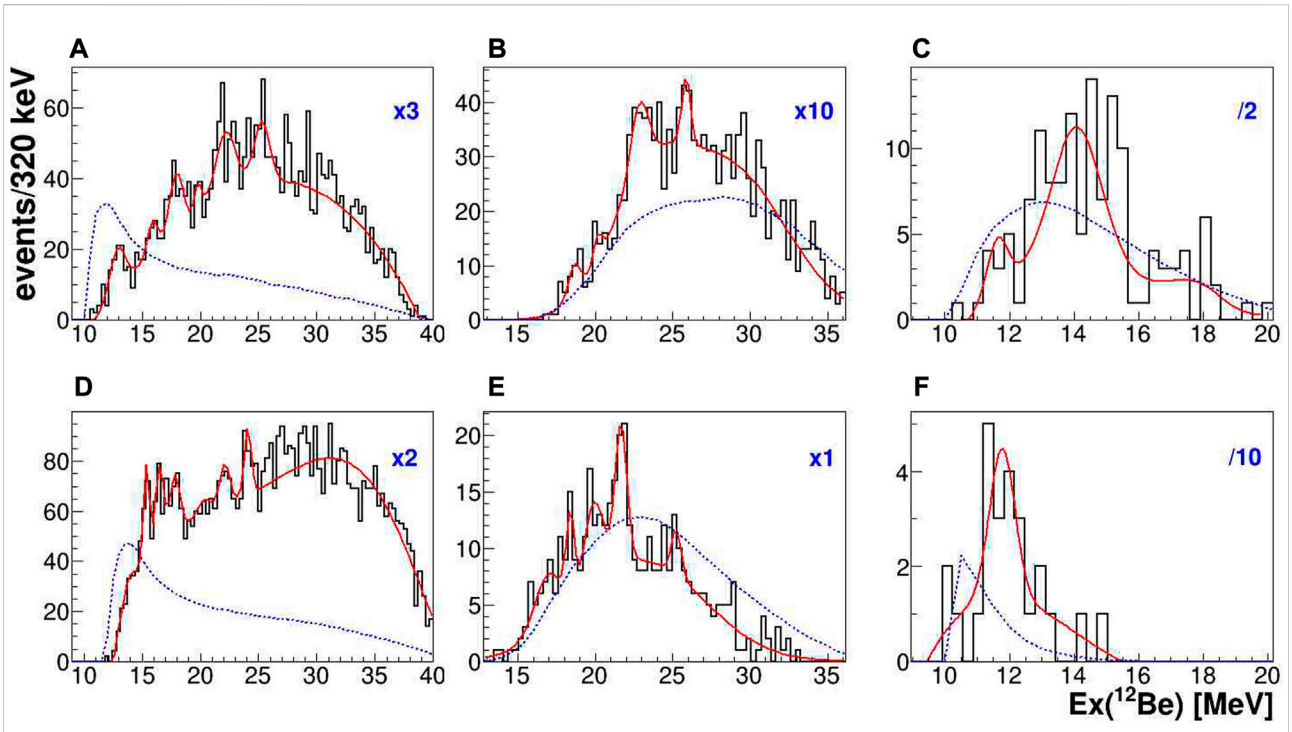

FIGURE 5
Examples of the ^{12}Be excitation energy spectra for the ^{6}He + ^{6}He decay. Spectra are reconstructed for the ^{4}He + ^{6}He coincidences for dT = 3 and undetected ^{6}He in the ground state **(A)**; ^{6}He + ^{6}He coincidences for dT = 3 **(B)** and dT = 1 **(C)**; ^{4}He + ^{6}He coincidences for dT = 3 and undetected ^{6}He in the first excited state **(D)**; ^{6}He + ^{6}He coincidences for dT = 2 **(E)** and dT = 0 **(F)**. Solid red curves are results of the best fit using Gaussian curves for the peaks on the estimated background. Dotted blue curves represent the detection efficiency calculated by Monte Carlo simulations multiplied by the labeled factor.

data. In the ^{4}He + ^{6}He + ^{6}He triple coincidence events, only the ^{10}Be states were observed while in the ^{4}He + ^{4}He + ^{8}He triple coincidences, in addition to the more intense ^{8}Be states, also two ^{12}Be states were observed.

3 Results and discussion

Here are presented some typical spectra from the full set of the results given in [29] which best illustrate the results obtained for the ^{12}Be excited states. The first set of spectra presented in Figure 3 show correlation plots used to identify the events produced in the various possible reaction exit channels—Catania plots. On these plots are presented selected coincidence events of identified reaction product pairs relevant for the study of the ^{12}Be excited states. In all of the cases presented here, reaction products were detected in the telescopes on opposite sides of the beam trajectory (dT = 3). The nominal relative azimuthal angle between detected reaction products of 180° was used initially in the event reconstruction and this led to a small shift in the corresponding Q-value, which in the worst case was 500 keV. The spectra A and C correspond to the data for the ^{6}He + ^{6}He decay of the ^{12}Be excited states, that is, the reaction (2) with a Q-value of 2.253 MeV. The spectra B and D are for the ^{4}He + ^{8}He decay and reaction (1) with Q = 3.402 MeV. In all of the spectra, red lines mark the loci associated with the reaction on ^{7}Li, blue dashed lines are for the reaction on ^{6}Li, and black dotted lines are for the reaction on ^{19}F. Additional red and black lines in plot C correspond to the undetected ^{6}He in its first excited state at 1.8 MeV for the reaction on ^{7}Li and to the ^{18}O in its first excited state at 1.99 MeV for the reaction on ^{19}F, respectively (the Q-values are more negative for the excited state than those for the ground state reaction). In plot D, there appears an intense locus of the events having a large slope and marked with purple line, which corresponds to the reaction on the hydrogen content of the target. These spectra show that for the ^{6}He + ^{6}He, ^{4}He + ^{8}He ,and ^{4}He + ^{6}He coincidence events, clean identification of events originating from the reaction on ^{7}Li is possible, while for the ^{4}He + ^{4}He case, the selected events may contain some background contributions from other reactions, even if events at the crossing with intense hydrogen locus were excluded from further analysis.

The 2D excitation energy correlation plots for identification of the excited states in the composite systems, made of various pairs of the final reaction products, are presented in Figure 4. For the selected events of the particular reaction, the excitation

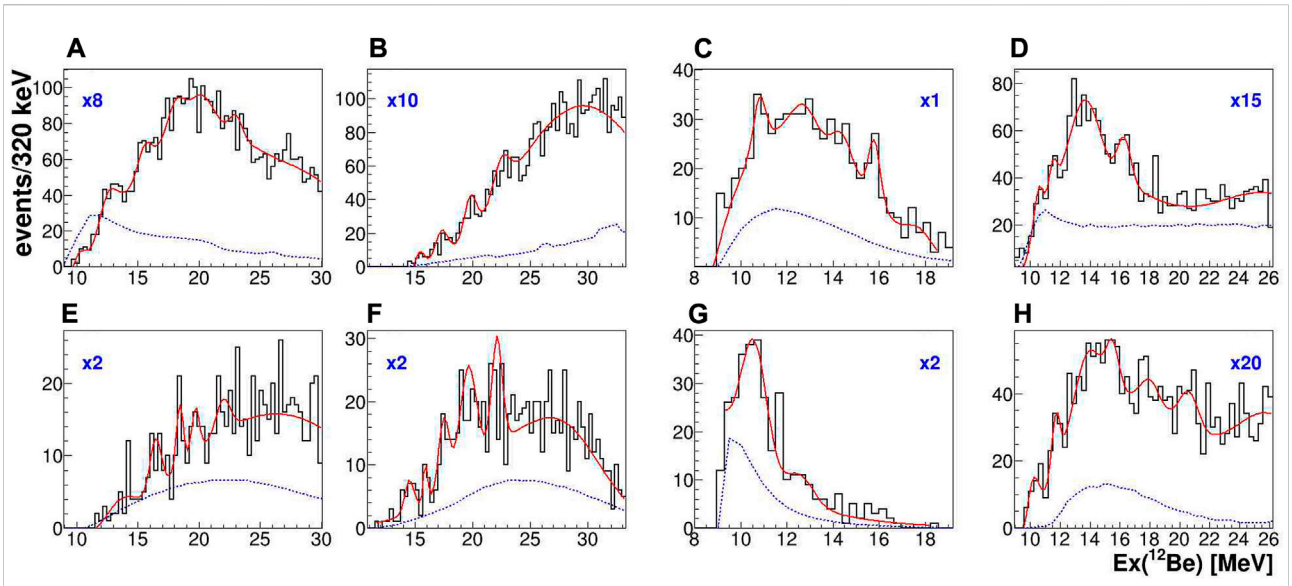

FIGURE 6
Examples of the ^{12}Be excitation energy spectra for the ^{4}He + ^{8}He decay. Spectra are reconstructed for the ^{4}He + ^{8}He coincidences for dT = 3 and ^{8}He paired with undetected ^{4}He **(A)** and detected ^{4}He **(B)**; ^{4}He + ^{8}He coincidences for dT = 1 and ^{8}He paired with detected ^{4}He **(C)**; ^{4}He + ^{4}He coincidences for dT = 3 and summed contributions of the ^{8}He paired with undetected and detected ^{4}He **(D)**; ^{4}He + ^{8}He coincidences for dT = 2 and ^{8}He paired with undetected ^{4}He **(E)** and detected ^{4}He **(F)**; ^{4}He + ^{8}He coincidences for dT = 0 and ^{8}He paired with detected ^{4}He **(G)**; ^{4}He + ^{4}He coincidences for dT = 2 and summed contributions of the ^{8}He paired with undetected and detected ^{4}He **(H)**. Solid red curves are results of the best fit using Gaussian curves for the peaks on the estimated background. Dotted blue curves represent the detection efficiency calculated by Monte Carlo simulations multiplied by the labeled factor.

energy spectra are reconstructed: spectra A, B, C, and D are for selected events associated with the ^{6}He + ^{6}He decay, while plots E, F, G, and H are for the ^{4}He + ^{8}He decay of the ^{12}Be states. Spectra are presented for the ^{4}He + ^{6}He coincidences in opposite telescopes (dT = 3), for undetected ^{6}He in the ground state (A) and the first excited state at 1.8 MeV (B), ^{6}He + ^{6}He coincidences for dT = 3 (C) and dT = 1 (D) case, ^{4}He + ^{4}He coincidences for dT = 3 (E) and dT = 2 (F) case, and ^{4}He + ^{8}He coincidences for dT = 3 (G) and dT = 1 (H) case. In the spectra A, B, and C, the intense loci correspond to the ^{10}Be states but also loci associated with the ^{12}Be states are visible. In the spectra E and F, the strongest loci are for the ^{8}Be states which are observed as diagonal loci on the spectra G and H. In these spectra, the ^{12}Be states can be also observed.

These 2D correlation plots were used to produce the final ^{12}Be excitation energy spectra as projections on the ^{12}Be axis, excluding in these projections regions with intense contributions of the ^{8}Be/^{10}Be states. The ^{12}Be excitation energy spectra obtained for the ^{6}He + ^{6}He and ^{6}He + ^{6}He*(1.8 MeV) decays are presented in Figure 5, and the spectra for the ^{4}He + ^{8}He decay are presented in Figure 6. Figure 5 presents spectra for the ^{4}He + ^{6}He coincidences for dT = 3 case and undetected ^{6}He in the ground state (A), ^{6}He + ^{6}He coincidences for dT = 3 (B) and dT = 1 (C), ^{4}He + ^{6}He coincidences for dT = 3 and undetected ^{6}He in the first excited state (D), and ^{6}He + ^{6}He coincidences for dT = 2 (E) and dT = 0 (F). Figure 6 presents spectra for the ^{4}He + ^{8}He coincidences for dT = 3 and ^{8}He paired with undetected ^{4}He (A) and detected ^{4}He (B); ^{4}He + ^{8}He coincidences for dT = 1 and ^{8}He paired with detected ^{4}He (C); ^{4}He + ^{4}He events for dT = 3 and summed contributions of the ^{8}He paired with undetected and detected ^{4}He (D), ^{4}He + ^{8}He for dT = 2 and ^{8}He paired with undetected ^{4}He (E) and detected ^{4}He (F), ^{4}He + ^{8}He for dT = 0 and ^{8}He plus detected ^{4}He (G), and ^{4}He + ^{4}He events for dT = 2 and summed contributions of the ^{8}He with undetected and detected ^{4}He (H). In these figures, solid red curves are the results of the best fit using Gaussian curves for the peaks on the background represented by the polynomial function and, in some spectra, broad Gaussian function at the highest excitations. Dotted blue curves present detection efficiency calculated by Monte Carlo simulations multiplied by the labeled factor.

As already mentioned earlier, in all of the event selection processes, rigorous criteria were used in the attempt to minimize background contributions and filter as clean data as possible. This procedure significantly reduced the final number of accepted events and resulted in a small number of counts in the peaks associated with the ^{12}Be excited states. Due to the limitations of the experimental setup, also the resolution in the excitation energy is rather low. The results of the simulations provided the estimates of experimental excitation energy resolution as follows: for excitation energy 3 MeV above the decay threshold for dT = 1 events FWHM = 950 keV; for

TABLE 1 ^{12}Be excited states observed in the ^{6}He+^{6}He decay. Observation of a clear peak is labeled with ●, indication of a peak with ◦, and a possible peak obscured by the background or other peaks, or affected by the detection efficiency, with ×. Tentative states are in parenthesis.

^{6}He+^{6}He ↓ ‖ Ex [MeV] →	(11.7)	13.5	(16.5)	18.5	(20.0)	22.5	25.4
^{7}Li(^{9}Li, ^{4}He^{6}He)$_{dT=3}$^{6}He (23)	×	●	◦	●	◦	●	●
^{7}Li(^{9}Li, ^{6}He^{6}He)$_{dT=3}$^{4}He (12)				●	◦	●	●
^{7}Li(^{9}Li, ^{6}He^{6}He)$_{dT=2}$^{4}He (12)			◦	●	●	●	◦
^{7}Li(^{9}Li, ^{6}He^{6}He)$_{dT=1}$^{4}He (12)	◦	●	×				
^{7}Li(^{9}Li, ^{6}He^{6}He)$_{dT=0}$^{4}He (12)	●						

TABLE 2 ^{12}Be excited states observed in the ^{6}He+^{6}He*(1.8 MeV) decay. Observation of a clear peak is labeled with ●, indication of a peak with ◦, and possible peak obscured by the background or other peaks, or affected by the detection efficiency, with ×. Tentative states are in parenthesis.

^{6}He+^{6}He* ↓ ‖ Ex [MeV] →	15.4	16.5	17.8	22.1	24.0
^{7}Li(^{9}Li, ^{4}He^{6}He)$_{dT=3}$^{6}He* (23)	●	●	●	●	●

excitation energy 6 MeV above the decay threshold for dT = 2 events FWHM = 1,050 keV and for dT = 3 FWHM = 750 keV; for excitation energy 10 MeV above the threshold for dT = 2 FWHM = 1,150 keV and for dT = 3 FWHM = 820 keV. It should be mentioned that the same problems, limited data statistics, poor resolution, and large background, can be seen in all published results on the helium decays of the ^{12}Be states.

The ^{12}Be states observed in this work that decay to ^{6}He + ^{6}He are listed in Table 1, to ^{6}He + ^{6}He*(1.8 MeV) in Table 2, and to ^{4}He + ^{8}He in Table 3. In these tables, all datasets on the ^{7}Li target in which the particular decay channel can be observed are listed. For some datasets, it was not possible to separate different reaction exit channels, for example, in the ^{4}He + ^{6}He coincidences, for dT = 1, 2 cases, the events of the ^{6}He decays into the ground and the first excited state of the undetected ^{6}He cannot be separated. Also, the datasets for which the relative energy of the reaction product pair corresponding to the ^{12}Be is at very high excitation are not considered, for example, the ^{4}He + ^{6}He coincidences for dT = 0. The dataset labels indicate the reaction exit channel in the form t(p,1 2)3, the identifier of the pair of detector segments in which reaction products were detected (dT = 0,1,2,3), and a pair of the reaction products forming the ^{12}Be state. For each dataset and each observed ^{12}Be state, the level of confidence of the peak observation is indicated: clear peak, indication of the peak (one with a small number of counts), and possible peak (one seen in other datasets, but in this case, it is obscured by contributions from the background or other peaks or affected by the detection efficiency). An empty position in the table means that the particular dataset does not cover the ^{12}Be excitation energy interval of the peak observed in other datasets. The peaks with clear observation in, at least, two datasets are considered as the ^{12}Be states. Other peaks in the tables, all of them satisfying aforementioned criteria for a candidate for the state, are considered as tentative states. Estimated uncertainty in their positions is ±250 keV for excited states from the decay thresholds to 14 MeV in excitation and ±400 keV for the states at higher excitations.

Taking into account the quoted uncertainty in the excitation energy and experimental resolution, most of the observed states can be associated with the states seen in the previous experiments [12–18]. The ^{12}Be decay to ^{6}He + ^{6}He*, where one ^{6}He is in its

TABLE 3 ^{12}Be excited states observed in the ^{4}He+^{8}He decay. Observation of a clear peak is labeled with ●, indication of a peak with ◦, and a possible peak obscured by the background or other peaks, or affected by the detection efficiency, with ×. Tentative states are in parenthesis.

^{4}He+^{8}He ↓ ‖ Ex [MeV] →	10.3	(12.1)	13.8	15.6	17.5	(19.8)	(22.3)
^{7}Li(^{9}Li, ^{4}He^{8}He)$_{dT=3}$^{4}He (23)	×	×	●	◦	◦	◦	◦
^{7}Li(^{9}Li, ^{4}He^{8}He)$_{dT=2}$^{4}He (23)			◦	●	●	●	◦
^{7}Li(^{9}Li, ^{4}He^{8}He)$_{dT=3}$^{4}He (12)				◦	●	◦	◦
^{7}Li(^{9}Li, ^{4}He^{8}He)$_{dT=2}$^{4}He (12)			◦	◦	◦	◦	◦
^{7}Li(^{9}Li, ^{4}He^{8}He)$_{dT=1}$^{4}He (12)	●	◦	◦	●	◦		
^{7}Li(^{9}Li, ^{4}He^{8}He)$_{dT=0}$^{4}He (12)	●	◦					
^{7}Li(^{9}Li, ^{4}He^{4}He)$_{dT=3}$^{8}He (13 + 23)	◦	◦	●	●	×	×	×
^{7}Li(^{9}Li, ^{4}He^{4}He)$_{dT=2}$^{8}He (13 + 23)	◦	◦	◦	◦	●	◦	×

TABLE 4 ^{12}Be states observed in this work in the three helium-cluster decays. Tentative states are in parenthesis. The states observed in the previous studies are in bold.

Decay ‖E_x[MeV]								
^{6}He+^{6}He		**(11.7)**	**13.5**	**(16.5)**	**18.5**	(20.0)	**22.5**	**25.4**
^{6}He+^{6}He*			15.4	16.5	17.8		22.1	24.0
^{4}He+^{8}He	**10.3**	**(12.1)**	**13.8**	**15.6**	**17.5**	**(19.8)**	(22.3)	

first excited state at 1.8 MeV and with $J^\pi = 2^+$, is observed for the first time in this work. Two of the observed five states in this decay channel most likely correspond to the states decaying to the ground state channel ^{6}He + ^{6}He, while the other two may correspond to the states decaying into the ^{4}He + ^{8}He decay channel.

At the low excitations, from the ^{4}He + ^{8}He decay threshold at 8.96 MeV, and the ^{6}He + ^{6}He threshold at 10.11 MeV, up to 14 MeV, states are observed in the ^{4}He + ^{8}He decay channel at 10.3 and 13.8 MeV, as well as the possible state at 12.1 MeV. The 13.8 MeV state is also observed in the spectra for the ^{4}He + ^{4}He + ^{8}He triple coincidence events. In the ^{6}He + ^{6}He decay channel, a state is observed at 13.5 MeV and indications for the state at 11.7 MeV are found. The 10.3 MeV state was observed in [16, 17], where its spin 0^+ was deduced and it was proposed as the band head of the ^{4}He + ^{8}He rotational band. In the same work, two other states at 12.1 and 13.6 MeV were observed, for the 13.6 MeV state, its spin/parity 4^+ was deduced and it was claimed that these states are 2^+ and 4^+ members of the rotational band with very high deformation. The 12.1 MeV state was observed in [12, 13], as well as a state around 14 MeV. The broad peak around 13.6 MeV was observed in [15]. In [12, 13], a spin of 4^+ was deduced for the 12.1 MeV and 14 MeV states. The states which may correspond to here propose 11.7 MeV state in the ^{6}He + ^{6}He channel were observed in [14, 16, 17], while the state around 13.5 MeV was observed in [12–17]. It is likely that the 13.5 MeV state in the ^{6}He + ^{6}He channel is the same state seen at 13.8 MeV in the ^{4}He + ^{8}He channel. The experimental FWHM values obtained in fits of the spectra in this work support this claim.

In the ^{12}Be excitation energy ranging from 14 MeV to 19 MeV, in this work, in the ^{4}He + ^{8}He decay channel, the states are observed at 15.6 and 17.5 MeV. The 17.5 MeV state also appears in the spectra for the ^{4}He + ^{4}He + ^{8}He triple coincidence events. In this decay channel, the states were observed close to 15.6 MeV in [12, 13, 15]. In [12, 13], also, the states at 17.4 and 18.2 MeV are reported. The peak around 17.5 MeV can be seen in this decay channel in spectra published in [15]. In the ^{6}He + ^{6}He decay channel, a state is observed in this work at 18.5 MeV and indications for the state at 16.5 MeV are found. In [12, 13], the states were reported at 16.1, 17.8, and 18.6 MeV, all with deduced $J^\pi = 6^+$, while the spectra published in [15] show peak around 18 MeV. In the ^{6}He + ^{6}He*(1.8 MeV) decay channel, the states are observed at 15.4, 16.5, and 17.8 MeV. The 15.4 and 17.8 MeV states may correspond to the 15.6 and 17.5 MeV states observed in the ^{4}He + ^{8}He channel. The 16.5 MeV state is the only one of three observed states which may be associated to the ^{6}He ground state decay channel.

This decay scheme is different than the one observed in the ^{10}Be states. It was observed in [35, 36] that the same ^{10}Be states decay to the ground and the first excited state of ^{6}He, both for the states with neutrons in pure σ orbitals and with a mixture of σ and π orbitals. It is not straightforward to link helium-cluster decay modes of these two nuclei, because ^{12}Be is a more complex system with one proposed cluster, ^{8}He, having neutron halo structure. If this difference in the ^{6}He decay modes is not the result of limited quality of the presented ^{12}Be experimental results, then it is related to the structural differences of these two Be isotopes due to bonding of additional two neutrons around the α—α cores.

At higher ^{12}Be excitations, from 19 to 25 MeV, in this work, in the ^{6}He + ^{6}He decay channel, the states are observed at 22.5 and 25.4 MeV and in the ^{6}He + ^{6}He*(1.8 MeV) channel, at 22.1 and 24.0 MeV. There are also indications for the state at 20.0 MeV in the ^{6}He ground state decay channel. The ^{6}He*(1.8 MeV) decaying state at 22.1 MeV may correspond to the state observed in the decay to the ^{6}He ground state at 22.5 MeV. The state at 24.0 MeV does not have its counterpart in other two decay channels. In the ^{4}He + ^{8}He decay channel, a state is observed at 19.8 and indications for the state at 22.3 MeV are found. It is plausible to correlate these states to the ones seen in the ^{6}He decay channels. In this excitation energy range, states are reported [12, 13] at 19.4 and 20.7 MeV in the ^{4}He + ^{8}He channel and at 19.3, 20.9, 22.8, 24.0, and 25.1 in the ^{6}He + ^{6}He channel.

The summary of the ^{12}Be states observed in this work to decay by the helium-cluster emission is given in Table 4. All observed states in the three decay channels examined are listed, with tentative states in parenthesis. The states which correlate with previously observed states are in bold. The states observed in the ^{6}He + ^{6}He decay channel are at 13.5, 18.5, 22.5, and 25.4 MeV, and indications for additional states at 11.7, 16.5, and 20.0 MeV are found. Five states are observed in the ^{6}He + ^{6}He*(1.8 MeV) decay channel, at 15.4, 16.5, 17.8, 22.1, and 24.0 MeV. In the ^{4}He + ^{8}He channel, states are observed at 10.3, 13.8, 15.6, and

TABLE 5 Decay threshold energies of relevant decay channels for the ^{12}Be helium-decaying states.

Decay	^{11}Be + n	^{10}Be+2n	^{4}He+^{8}He	^{6}He+^{6}He	^{9}Be+3n	^{6}He+^{6}He*	^{8}Be+4n	^{9}Li+^{3}H
E_{thr} [MeV]	3.17	3.67	8.96	10.11	10.49	11.91	12.15	14.83

17.5 MeV, and indications for the states at 12.1, 19.8, and 22.3 MeV are found.

The ^{4}He + ^{8}He* decay, with ^{8}He in its first excited state, was examined in the ^{4}He + ^{4}He coincidences, but due to the large background in this dataset (Figure 3D) and the large width of the ^{8}He excited state, there was no signature of this decay of the ^{12}Be states. The data analysis for possible ^{9}Li + ^{3}H decay did not provide any indication for this decay of the ^{12}Be states. This decay channel was studied only in [15], and the result was structureless spectrum with an indication of a state at 17.7 MeV. In these sets of data, the known excited states of ^{7}Li decaying into ^{4}He + ^{3}H and excited states of ^{13}B are observed. The ^{13}B results will be presented in a separate publication. Data analysis for the neutron decay to the ^{11}Be ground and first excited state is also performed but due to the detector array geometry, the ^{11}Be + ^{4}He coincidence data scan very high excitation energies in ^{12}Be and provide the structureless spectrum. The present experimental data cannot provide information on the spin and parity of the observed states, not only due to low statistics and unfavorable resolution but also due to the non-zero spin projectile and target nuclei (both ^{9}Li and ^{7}Li have $J^{\pi} = 3/2^{-}$). The only hint on the possible spin/parity of the observed states is coming from its decay mode: the states decaying into the ^{6}He + ^{6}He must have even spin and positive parity (0^{+}, 2^{+}, 4^{+} *etc.*) because of identical 0^{+} constituents, while the states decaying into the ^{4}He + ^{8}He must be natural parity states (0^{+}, 1^{-}, 2^{+}, 3^{-} *etc.*) as both constituents are 0^{+} nuclei.

An attempt was made in the data analysis to get some hint on the reaction mechanisms of the ^{9}Li + ^{7}Li reaction which populates the helium-decaying states in ^{12}Be. It was already mentioned that the expected main reaction mechanisms are the triton transfer from ^{7}Li to ^{9}Li and the t + 2n transfer from ^{9}Li to ^{7}Li. For this reason, the detector array geometry was optimized to increase the detection efficiency for reaction products of these transfer reactions using AUSA software tools [37]. Unfortunately, this detector geometry also optimizes detection of the background events from the decays of the ^{8}Be states into ^{4}He + ^{4}He and of the ^{10}Be states into ^{4}He + ^{6}He. These ^{8,10}Be* helium-cluster decays were populated in much simpler transfer reactions with larger cross sections: the proton, for the ^{8}Be, and triton, for the ^{10}Be, transfer from ^{9}Li to ^{7}Li, and the proton transfer from ^{7}Li to ^{9}Li for ^{10}Be. In the cluster transfer reactions, the residual part of the nucleus weakly interacts in the reaction and will slightly change its state of motion. Thus, if a triton is transferred from the ^{7}Li target to ^{9}Li beam to form ^{12}Be, recoil α from ^{7}Li will have small kinetic energy. Similarly, if the t + 2n are transferred from ^{9}Li beam to ^{7}Li, the recoil α from ^{9}Li will slightly change the velocity it had as a part of the beam particle. With kinematical consideration of the momentum of the recoil α-particle, it was possible to select events most likely originating from these transfer reactions. Indeed, it is found that all observed helium-decaying ^{12}Be states are also seen in these subsets of the data. However, it is also found that for some of these states, for which the detection efficiency permitted detection of corresponding events and which are not obstructed by events originated in decays of the ^{8,10}Be states, the recoil α-particles have a broad range of the momentum. This would imply that the helium-decaying ^{12}Be states were also produced in reactions such as fusion followed by α-particle emission. Unfortunately, low data statistics and unfavorable energy and angular resolution are prohibiting detailed analysis of the reaction process. It should be mentioned that non-observation of the ^{12}Be states decaying into the ^{9}Li + ^{3}H channel implies that there is no resonant contribution in the triton transfer process from ^{7}Li to ^{9}Li.

4 Conclusion

An experimental study of the ^{12}Be excited states decaying into ^{4}He + ^{8}He and ^{6}He + ^{6}He has been performed using the ^{9}Li + ^{7}Li $\rightarrow \alpha + {}^{12}$Be* $\rightarrow \alpha + \alpha + {}^{8}$He and ^{9}Li + ^{7}Li $\rightarrow \alpha + {}^{12}$Be* $\rightarrow \alpha + {}^{6}$He + ^{6}He reactions. The ^{9}Li beam of energy of 74.8 MeV and LiF targets of thickness $\approx$ 1 mg/cm^{2} were used in the experiment. A large solid angle silicon strip detector array assembled of six wedge-shaped detector telescopes was used to detect reaction products. The reaction products were identified using the ΔE–E technique. The data analysis consisted of a sequence of event reconstruction and event selection procedures aimed to reject events originating from the background processes and to achieve a clean set of events for further analysis. In each step, rigorous criteria for selection of the events were applied and quality checks were performed by comparing the results obtained with the well-known properties of the nuclei involved in the considered reactions.

The ^{12}Be excitation energy spectra were reconstructed for two possible helium-cluster decay channels: for the ^{6}He + ^{6}He decay, the ^{4}He + ^{6}He and ^{6}He + ^{6}He coincidences and for the ^{4}He + ^{8}He decay, the ^{4}He + ^{8}He and ^{4}He + ^{4}He coincidences were analyzed. In the ^{4}He + ^{6}He + ^{6}He exit channel, strong background contributions from the ^{10}Be states decaying into the ^{4}He + ^{6}He were observed. The ^{8}Be excited states decaying into two

α-particles produced a strong background in the ^{12}Be excitation energy spectra for the ^{4}He + ^{8}He decay. The ^{8,10}Be* nuclei were produced by much simpler reaction mechanisms than ^{12}Be*, so the cross sections for their production are much larger than the ones for the ^{12}Be*. Contributions of the strongest ^{8,10}Be states were excluded from the final ^{12}Be excitation energy spectra. The datasets of various ^{x}He + ^{y}He coincidence events detected in all possible pairs of the detector array segments were analyzed, and the results are presented separately. The excitation energy spectra obtained have significant background contributions, rather low resolution and observed peaks mostly have limited data statistics, but the same problems can be seen in all published results on the helium decays of the ^{12}Be states. A peak in the excitation energy spectrum is considered as a candidate for the ^{12}Be excited state if it was seen in corresponding 2D correlation plots of excitation energies in at least two independent datasets and if the fit parameters of the state agreed for different datasets. The data for the ^{6}He + ^{6}He*(1.8 MeV) decay could only be separated from the data for the ^{6}He ground state decay channel for one dataset, the dT = 3 ^{4}He + ^{6}He coincidences, and this is the only exception from these criteria. The candidate states are further filtered by the criterion of clean observation in at least two independent datasets, the candidate states which did not pass this criterion are considered as tentative states.

The results are the ^{12}Be excitation energy spectra with the following observed excited states: 1) 13.5, 18.5, 22.5, and 25.4 MeV states, and tentative states at 11.7, 16.5, and 20.0 MeV in the ^{6}He + ^{6}He decay channel; 2) 15.4, 16.5, 17.8, 22.1, and 24.0 MeV states decaying into ^{6}He + ^{6}He*(1.8 MeV, $J^{\pi} = 2^{+}$); and 3) the states at 10.3, 13.8, 15.6, and 17.5 MeV, and tentative states at 12.1, 19.8, and 22.3 MeV, decaying into ^{4}He + ^{8}He. The estimated uncertainty in their positions is ±250 keV for excited states from the decay threshold energies up to 14 MeV and ±400 keV for the states at higher excitations. Most of the observed states were seen in the previous experiments. The ^{6}He + ^{6}He*(1.8 MeV) decay of the ^{12}Be states is observed for the first time. Two of the five states observed in this decay channel most likely also decay to the ground state channel ^{6}He + ^{6}He, while two may correspond to the ^{4}He + ^{8}He decaying states. The 24.0 MeV state does not have a counterpart in the other two decay channels. The states around 13.5 and 20.0 MeV decay to the ^{6}He + ^{6}He and ^{4}He + ^{8}He channels, while the state around 22.3 MeV decays to all three decay channels examined. The experimental results presented here cannot provide information on the spin and parity of the observed states, due to the non-zero spin projectile and target nuclei. The decay modes of the observed helium-cluster decaying states provide limited information on their possible spin/parity as the states decaying into the ^{6}He + ^{6}He must have even spin and positive parity (0^{+}, 2^{+}, 4^{+}, *etc.*), while the states decaying into ^{4}He + ^{8}He must be natural parity states (0^{+}, 1^{-}, 2^{+}, 3^{-}, *etc.*).

The data analysis for the ^{4}He + ^{8}He* decay with ^{8}He in its first excited state, for the ^{9}Li + ^{3}H decay and for the neutron decays to the ^{11}Be ground and first excited state for excitations higher than 25 MeV, was also performed, but the results obtained do not provide evidence for these decays of the ^{12}Be excited states. The limited quality of obtained results and the reduced reaction phase space explored in the final dataset, due to the applied rigorous event selection criteria, do not permit detailed analysis of the reaction mechanism populating the helium-cluster decaying ^{12}Be states, but simple considerations of the momentum of recoil α-particle imply that various complex reaction mechanisms, from triton transfer to compound nucleus reactions, may populate these states.

In the presented experimental work, it was not possible to identify proposed rotational bands because this measurement could not provide information on the spin, parity, and partial decay widths of the observed ^{12}Be states. Even if the presented results provide limited evidence for the molecular structure in ^{12}Be, they are one important step forward in the understanding of its structure because of the new spectroscopy information and the observation of the new decay mode of the states. Consequently, this advance in understanding of the ^{12}Be structure may improve the understanding of the structure of light neutron-rich nuclei in general. This experiment is the first measurement aimed to study ^{12}Be by use of the complex nuclear reactions to populate exotic cluster structures in the neutron-rich light nuclei. The observation of the helium-cluster decays of the ^{12}Be states validates this approach and opens the path for future studies of other neutron-rich light nuclei (such as ^{14,15}B and ^{15,16,17}C) by the use of re-accelerated neutron-rich ion beams such as the ^{9}Li beam at the ISAC-II facility at TRIUMF. The observed helium-cluster decaying ^{12}Be excited states are in agreement with results of the previous experiments, particularly [12, 13, 16, 17], all performed by the use of breakup after inelastic excitation of the ^{12}Be fragmentation beams. These new results show that previous results are not artifacts of the applied experimental technique. It is evident that in the excitation energy interval from 10 to 25 MeV, there are the ^{12}Be excited states decaying into the ^{4}He + ^{8}He and ^{6}He + ^{6}He, and, as it is presented here for the first time, into the ^{6}He + ^{6}He*(1.8 MeV) channel. The observation of the states at these high excitations with these exotic decay properties is strongly supporting the molecular structure in the ^{12}Be. An inspection of the decay threshold energies in ^{12}Be (Table 5) leads to the conclusion that these states should have some peculiar property which inhibits their decay into the ^{11}Be + n and ^{10}Be + 2n channels, most probable decay modes for states at the excitations with very high density of the n/2n states and enables their decay into the helium-decaying channels. This peculiar property should be their special structure, most likely the cluster molecular structure of four neutrons orbiting two α-clusters, as it is proposed in a number of theoretical studies [10, 19–24].

Evidently, new experimental efforts are needed to uncover the structure of ^{12}Be, one of the key nuclei to improve the

knowledge of the clustering in the neutron-rich nuclei. For example, measurements of the reactions studied in this work with an improved detector array with better angular resolution and larger angular coverage could provide high-quality data which will result in improved characterization of the states, including the partial widths for the various decay channels, the important information to confirm the molecular nature of the states. The use of the large solid angle segmented neutron detector in these measurements would enable determination of the partial widths for various possible neutron-decay channels and would significantly enhance the knowledge of the ^{12}Be structure.

Data availability statement

The raw data supporting the conclusions of this article will be made available by the authors, without undue reservation.

Author contributions

NS and MF were spokespersons of the experiment S1620 at TRIUMF, they proposed and led the experiment. NV did simulations for the optimization of the experimental setup and analyzed the experimental data under mentorship of NS. All authors contributed to setup of the experiment and the measurements. NS prepared the first draft, the revised versions and the final version of the manuscript. All authors contributed to manuscript revisions and read and approved the submitted version.

Funding

This work has been supported in part by the Croatian Science Foundation under Project no. 7194 and Project no. IP-2018-01-1257, by the European Regional Development Fund for the "Center of Excellence for Advanced Materials and Sensing Devices" (Grant No. KK.01.1.1.01.0001) and for the Competitiveness and Cohesion Operational Programme (Grant No. KK.01.1.1.06), as well as by the European Union's Horizon 2020 research and Innovation programme under grant agreement No. 669014. Part of the work has been supported by the Natural Sciences and Engineering Research Council of Canada under grants SAPPJ-2019-00039 and SAPMR 2020-00004. AD acknowledges support provided by the Istituto Nazionale di Fisica Nucleare. TD acknowledges support provided by the UK Science and Technology Facilities Council.

Acknowledgments

The authors thank Antonio Massara from INFN LNS Catania for provided targets and Peter Machule from TRIUMF for technical support in the experimental setup. The authors acknowledge the technical support of the TRIUMF operations and beam delivery groups during the measurements. NS thanks Alison Laird from the University of York for providing an additional detector during the measurements. NS and NV thank Oliver Kirsebom and Michael Munch from the University of Aarhus for their support in running AUSA tools for the experimental setup optimization and Matko Milin from the University of Zagreb for fruitful discussions on the obtained results.

Conflict of interest

The authors declare that the research was conducted in the absence of any commercial or financial relationships that could be construed as a potential conflict of interest.

Publisher's note

References

1. Freer M, Horiuchi H, Kanada-En'yo Y, Lee D, Meissner U. Microscopic clustering in light nuclei. *Rev Mod Phys* (2018) 90:035004. doi:10.1103/RevModPhys.90.035004

2. von Oertzen W, Freer M, Kanada-En'yo Y. Nuclear clusters and nuclear molecules. *Phys Rep* (2006) 432:43–113. doi:10.1016/j.physrep.2006.07.001

3. Freer M. The clustered nucleus — Cluster structures in stable and unstable nuclei. *Rep Prog Phys* (2007) 70:2149–210. doi:10.1088/0034-4885/70/12/R03

4. von Oertzen W. Two-center molecular states in ^{9}B, ^{9}Be, ^{10}Be and ^{10}B. *Z Phys A — Hadrons Nuclei* (1996) 354:37–43. doi:10.1007/s002180050010

5. von Oertzen W. Dimers based on the $\alpha + \alpha$ potential and chain states of carbon isotopes. *Z Phys A - Particles Fields* (1997) 357:355–65. doi:10.1007/s002180050255

6. Freer M. Molecules in nuclei. *Comptes Rendus Physique* (2003) 4:475–87. doi:10.1016/S1631-0705(03)00050-1

7. Freer M, Casarejos E, Achouri L, Angulo C, Ashwood NI, Curtis N, et al. α:2n:α molecular band in ^{10}Be. *Phys Rev Lett* (2006) 96:042501. doi:10.1103/PhysRevLett.96.042501

8. Milin M, Zadro M, Cherubini S, Davinson T, DiPietro A, Figuera P, et al. Sequential decay reactions induced by a 18 MeV ^{6}He beam on ^{6}Li and ^{7}Li. *Nucl Phys A* (2005) 753:263–87. doi:10.1016/j.nuclphysa.2005.02.154

9. Soić N, Blagus S, Bogovac M, Fazinić S, Lattuada M, Milin M, et al. ^{6}He + α clustering in ^{10}Be. *Europhys Lett* (1996) 34:7–12. doi:10.1209/epl/i1996-00407-y

10. Ito M, Itagaki N, Sakurai H, Ikeda K. Coexistence of covalent superdeformation and molecular resonances in an unbound region of ^{12}Be. *Phys Rev Lett* (2008) 100:182502. doi:10.1103/PhysRevLett.100.182502

11. Korsheninnikov A, Nikolskii E, Kobayashi T, Aleksandrov D, Fujimaki M, Kumagai H, et al. Spectroscopy of ^{12}Be and ^{13}Be using a ^{12}Be radioactive beam. *Phys Lett B* (1995) 343:53–8. doi:10.1016/0370-2693(94)01435-F

12. Freer M, Angélique JC, Axelsson L, Benoit B, Bergmann U, Catford WN, et al. Exotic molecular states in ^{12}Be. *Phys Rev Lett* (1999) 82:1383–6. doi:10.1103/PhysRevLett.82.1383

13. Freer M, Angélique JC, Axelsson L, Benoit B, Bergmann U, Catford WN, et al. Helium breakup states in ^{10}Be and ^{12}Be. *Phys Rev C* (2001) 63:034301. doi:10.1103/PhysRevC.63.034301

14. Saito A, Shimoura S, Takeuchi S, Motobayashi T, Minemura T, Matsuyama YU, et al. Molecular states in neutron-rich beryllium isotopes. *Nucl Phys A* (2004) 738:337–41. doi:10.1016/j.nuclphysa.2004.04.057

15. Charity RJ, Komarov SA, Sobotka LG, Clifford J, Bazin D, Gade A, et al. Particle decay of ^{12}Be excited states. *Phys Rev C* (2007) 76:064313. doi:10.1103/PhysRevC.76.064313

16. Yang Z, Ye Y, Li Z, Lou J, Wang J, Jiang D, et al. Observation of enhanced monopole strength and clustering in ^{12}Be. *Phys Rev Lett* (2014) 112:162501. doi:10.1103/PhysRevLett.112.162501

17. Yang ZH, Ye YL, Li ZH, Lou JL, Wang JS, Jiang DX, et al. Helium-helium clustering states in ^{12}Be. *Phys Rev C* (2015) 91:024304. doi:10.1103/PhysRevC.91.024304

18. Freer M, Ashwood NI, Achouri NL, Catford WN, Curtis N, Delaunay F, et al. Elastic scattering of ^{8}He + ^{4}He and two-neutron transfer and the influence of resonances in ^{12}Be. *Phys Lett B* (2017) 775:58–62. doi:10.1016/j.physletb.2017.10.063

19. Maris P, Caprio MA, Vary JP. Emergence of rotational bands in *ab initio* no-core configuration interaction calculations of the Be isotopes. *Phys Rev C* (2015) 91:014310. doi:10.1103/PhysRevC.91.014310

20. Ito M, Ikeda K. Unified studies of chemical bonding structures and resonant scattering in light neutron-excess systems, $^{10,\ 12}$Be. *Rep Prog Phys* (2014) 77:096301. doi:10.1088/0034-4885/77/9/096301

21. Ito M. Formations of loose clusters in an unbound region of ^{12}Be. *Phys Rev C* (2012) 85:044308. doi:10.1103/PhysRevC.85.044308

22. Ito M, Itagaki N, Ikeda K. Cluster correlations for low-lying intruder states of ^{12}Be. *Phys Rev C* (2012) 85:014302. doi:10.1103/PhysRevC.85.014302

23. Dufour MPD, Nowacki F. Microscopic investigation of the ^{12}Be spectroscopy. *Nucl Phys A* (2010) 836:242–55. doi:10.1016/j.nuclphysa.2010.02.002

24. Kanada-En'yo Y, Horiuchi H. Cluster structures of the ground and excited states of ^{12}Be studied with antisymmetrized molecular dynamics. *Phys Rev C* (2003) 68:014319. doi:10.1103/PhysRevC.68.014319

25. Caurier E, Martínez-Pinedo G, Nowacki F, Poves A, Zuker AP. The shell model as a unified view of nuclear structure. *Rev Mod Phys* (2005) 77:427–88. doi:10.1103/RevModPhys.77.427

26. Lyu M, Yoshida K, Kanada-En'yo Y, Ogata K. Direct probing of the cluster structure in ^{12}Be via the α-knockout reaction. *Phys Rev C* (2019) 99:064610. doi:10.1103/PhysRevC.99.064610

27. Micron semiconductor (2022). YY1 design. Available from: http://www.micronsemiconductor.co.uk/product/yy1/.

28. Davinson T. Multistrip silicon detectors for studies with low energy RNBs. *Nucl Phys A* (2004) 746:188–94. doi:10.1016/j.nuclphysa.2004.09.145

29. Vukman N. PhD thesis: Clustering in neutron-rich light nuclei produced in reactions of ^{9}Li beam on LiF target. Zagreb, Croatia: University of Zagreb (2022).

30. Tilley D, Weller H, Cheves C. Energy levels of light nuclei A = 16-17. *Nucl Phys A* (1993) 564:1–183. doi:10.1016/0375-9474(93)90073-7

31. Tilley D, Cheves C, Godwin L, Hale G, Hofmann H, Kelley J, et al. Energy levels of light nuclei A=5, 6, 7. *Nucl Phys A* (2002) 708:3–163. doi:10.1016/S0375-9474(02)00597-3

32. Costanzo E, Lattuada M, Romano S, Vinciguerra D, Zadro M. A procedure for the analysis of the data of a three body nuclear reaction. *Nucl Instr Methods Phys Res Section A: Acc Spectrometers Detectors Associated Equipment* (1990) 295:373–6. doi:10.1016/0168-9002(90)90715-I

33. Dell'Aquila D (2021). UNISim MC framework Available from: https://github.com/dellaquilamaster/unisim-tool.

34. Tilley D, Kelley J, Godwin J, Millener D, Purcell J, Sheu C, et al. Energy levels of light nuclei. *Nucl Phys A* (2004) 745:155–362. doi:10.1016/j.nuclphysa.2004.09.059

35. Miljanic D, Soić N, Blagus S, Cherubini S, Costanzo E, Lattuada M, et al. ^{10}Be and molecular states. *Fizika B Zagreb* (2001) 10:235.

36. Soić N. *PhD thesis: Nuclear reactions with ^{7}Li and cluster structure of light nuclei*. Zagreb, Croatia: University of Zagreb (1999).

37. Aarhus Subatomic Group. AUSA software tools. (2017). Available from: https://git.kern.phys.au.dk/ausa.